

Article

# Mitigating Adverse Impacts of Increased Electric Vehicle Charging on Distribution Transformers

Akansha Jain  and Masoud Karimi-Ghartemani \* 

Department of Electrical and Computer Engineering, Mississippi State University,  
Mississippi State, MS 39762, USA

\* Correspondence: karimi@ece.msstate.edu

**Abstract:** As the world is transitioning to electric vehicles (EVs), the existing power grids are facing several challenges. In particular, the additional charging power demand may repeatedly overload the traditionally-sized distribution transformers and adversely impact their operational life. To address this challenge, this paper proposes an EV-based reactive power compensation strategy for transformer overloading mitigation. Specifically, a low-bandwidth centralized recursive controller is proposed to determine a set point for the EV's onboard charger's reactive power. Importantly, the proposed strategy is practically implementable in existing distribution grids as it does not rely on smart grid infrastructure and is stable under potential communication delays and partial failures. This paper discusses the controller's structure, design, and stability in detail. The proposed solution is tested with a realistic secondary distribution system considering four different EV charging scenarios with both Level 1 and Level 2 residential EV charging. Specifically, IEEE Standard C57.91-2011 is used to quantify the impact of EV charging on the transformer's life. It is shown that with the proposed method, transformer overloading is significantly reduced, and the transformer's life improves by an average of 47% over a year in all four scenarios.

**Keywords:** electric vehicles; distribution transformer; V2G; reactive power compensation; transformer aging



Citation: Jain, A.;

Karimi-Ghartemani, M. Mitigating Adverse Impacts of Increased Electric Vehicle Charging on Distribution Transformers. *Energies* **2022**, *15*, 9023. <https://doi.org/10.3390/en15239023>

Academic Editors: Komla A. Folly and N Kumarappan

Received: 18 October 2022

Accepted: 22 November 2022

Published: 29 November 2022

**Publisher's Note:** MDPI stays neutral with regard to jurisdictional claims in published maps and institutional affiliations.



**Copyright:** © 2022 by the authors. Licensee MDPI, Basel, Switzerland. This article is an open access article distributed under the terms and conditions of the Creative Commons Attribution (CC BY) license (<https://creativecommons.org/licenses/by/4.0/>).

## 1. Introduction

The world is shifting to electric vehicles (EVs). Despite its benefits, their charging process causes challenges to the power grid. Specifically, as most EV owners charge their vehicles at home, and the charging times often coincide with the peak load hours [1,2], the residential power demand is increasing significantly [3,4]. Consequently, legacy distribution equipment and devices are being pushed to their limits [5,6]. In particular, the distribution transformers may be overloaded by residential EV charging.

The impact of EV charging on distribution infrastructure has been reported in a number of studies. The impact of uncoordinated charging is discussed in [5], where active and reactive power data obtained from a local distribution station is utilized to quantitatively compare the effect of EV charging on distribution transformers and causing grid voltage asymmetry. A challenge with these types of analysis is obtaining realistic load, and EV profiles [7]. In [2], a solution for load and EV profile generation is proposed. While this technique ensures high modeling accuracy, it requires a base dataset to seed the stochastic model, which may not be readily available. Alternatively, probability distribution functions and the Monte-Carlo method for load modeling may be a useful trade-off between realistic modeling and the amount of prerequisite data [8,9]. In [10], smart meter data is used in a mixed technique to model the residential load on which the probabilistic EV charging profiles are overlaid randomly to study the impact of EV charging. The transformer's load profile obtained from real meter data or power flow studies can be used to estimate temperature and loss of life [11,12].

Frequent overloading can significantly accelerate the transformer's aging and cause a failure [13]. However, due to the significant cost involved, it is infeasible to simply upgrade all the distribution transformers [14]. Therefore, several methods have been proposed to mitigate this problem [15]. One strategy is passive demand-side management of EV charging through time-of-use (ToU) pricing [16]. The primary advantage of ToU strategies is their simplicity. It is shown in [17] that in several situations, ToU pricing is effective in shifting EV consumer behavior and flattening the load curve. However, it is crucial to accurately model both the non-EV and EV load profiles to determine the ToU pricing schedule [18,19]. To address this challenge, optimization, machine learning-based ToU pricing models have been proposed [20–22]. However, even correctly modeled ToU strategies may not be very effective at high EV penetration levels. Alternatively, active demand shaping techniques have been studied for managing EV charging loads [23–25]. These demand response techniques are based on actively regulating the charging interval of EVs based on optimal scheduling algorithms. As an example, in [26], a method is proposed to coordinate EV charging for transformer loss minimization based on load power flow. A similar technique to flatten the load profile based on smart charging points is presented in [27]. Furthermore, in addition to centralized controller based demand response techniques, decentralized solutions may also be used. In [28], authors propose a distributed charging control strategy considering distribution transformer energy loss, aging, and battery charging cost. In [29], authors propose a smart home energy management system to control EV charging times to reduce peak load. Active demand response based transformer overloading mitigation techniques may make the charging speed and duration unpredictable for the end user.

In this paper, reactive power compensation is proposed as a practical solution for minimizing the impact of EV charging on distribution transformers. Fundamentally, the proposed solution aims to reduce the distribution transformer's losses by reducing the reactive power flow through the transformer. Instead, the EVs supply local reactive power [30]. In this study, a realistic distribution system model with residential and EV loads and considering the effect of service lines and residential service drops are presented. A publicly available dataset is used for load and EV charging profiles [31]. Using this dataset, a baseline load profile is generated for a 24 h duration for various loading scenarios. Moreover, a baseline equivalent aging factor for the transformer is calculated according to IEEE C57.91-2011 standard [32]. This is used to quantify the impact of EV charging on transformer life. Furthermore, a reactive power compensation (RPC) based recursive controller is proposed to mitigate the adverse impact of EV charging on the transformer. The study considers a mix of both Level 1 and Level 2 EV charging [33]. It is shown that the proposed technique significantly improves the transformer life.

The key contributions of this work are as follows

1. The presented work quantifies the impact of Level 1 and Level 2 EV charging on the distribution transformer's life using a realistic system model and practical load EV charging data. This is used as a baseline for evaluating the effectiveness of the proposed reactive power compensation strategy.
2. The proposed research further presents a simple yet effective reactive power compensation strategy to mitigate the impact of EV charging on the distribution transformer. The primary advantages of the proposed technique are (1) convenience to the user, i.e., it does not impact their choice of time for charging and the charging speed, and (2) ease of implementation without requiring high bandwidth communication or numerous measurements. More precisely, it only requires reactive power measurements at the transformer site and EV connection status signals.
3. The research studies in detail the responses of the proposed controller on the distribution transformer and verifies the level of improvement achieved in transformer life. Moreover, the controller's stability and robustness to system communication delays and failures, as well as the impact of distribution cable impedance values, are studied.

## 2. Study System

In this section, the distribution system model used in this paper is introduced. It is subsequently used to quantitatively analyze the impact of EV charging on the distribution transformer's insulation life under various EV charging scenarios.

### 2.1. Study System Topology

The model used is based on a typical North American Distribution System [34]. The schematic of the system is shown in Figure 1. Since the study focuses on mitigating the impact of EV charging on the low-voltage distribution transformer life through secondary side compensation, a detailed model of the secondary distribution system is created, and the network upstream to the service transformer is ignored. For this study, the system considered has 20 load buses [35].

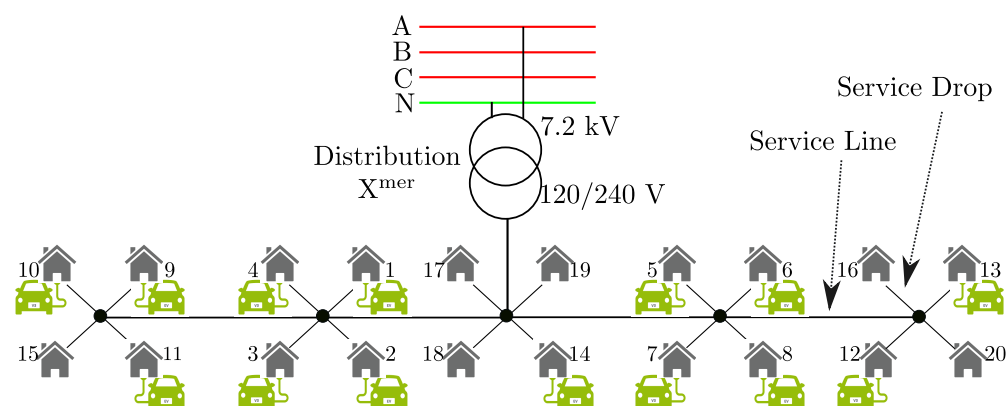


**Figure 1.** Schematic of secondary distribution system used for this study.

### 2.2. Residential Load Profile and EV Charging Data

The residential load data for this study is selected from [31], which provides active power profiles at 10 min intervals for 200 houses, of which 20 are randomly selected for this study. These load profiles are generated based on physical energy consumption models for various residential functions combined with a stochastic model for the individuals' activities [36]. In addition, the developed model is validated against actual meter data and shows low estimation error [37]. EV charging data is provided for both Level 1 and Level 2 charging. This EV data is generated by similarly combining stochastic models for the driver behavior, and driving profiles [38]. Level 1 charging power is taken to be at 1.92 kW and Level 2 at 6.6 kW [39]. Moreover, the same base user model is used both for load and EV modeling, which is critical for accuracy.

### 2.3. Other System Parameters

The distribution transformer's size is calculated as per the guidelines given in NEC Article 220 [40]. For the aforementioned data, in this study, a transformer rating of 45 kVA and a power factor (PF) of 0.9 lagging is selected based on [40–42]. The primary and secondary operating voltages of the transformer are 7.2 kV–120/240 V, respectively. The distribution transformer has a center-tapped secondary that provides two 120 V and a 240 V terminals. In a typical arrangement, a single pole-mounted distribution transformer may supply several homes. To supply a home, a triplex (with three conductors) service line connects the transformer outputs ( $L_1$ ,  $L_2$ ,  $N$ ) to the service pole closest to the home. The service-line self and mutual impedances for 125 ft cable are  $0.036 + j0.015$  and  $0.013 + j0.012$  Ohms respectively. The service drop is assumed to have the same cable type as the service line and is approximately 65 ft. Thus, service drop self and mutual impedances are half of the service-line impedances [12].

## 2.4. EV Charging Scenarios

The test scenarios considered in this study intend to assess various residential EV charging possibilities. The objective is to identify and analyze the impact of the additional demand on the distribution transformer's life under these scenarios. For Scenarios 1–3, 70% EV penetration (i.e., 14 EVs in 20 houses) is considered to represent a realistic high EV usage scenario.

### 2.4.1. Scenario 1

In this scenario, all the EVs are assumed to be charging at Level 1. This is a feasible scenario, especially for homes where the EVSE (Electric Vehicle Supply Equipment required for Level 2 charging) is either not installed or the home does not have the installation facility to begin with. For this study, all EVs have different charging profiles, which are randomly picked from the aforementioned dataset.

### 2.4.2. Scenario 2

To present the randomness of the residential EV charging levels, in this scenario, both Level 1 and Level 2 EV charging is considered, each at 50% of the total EV penetration. Again, all EVs considered have different charging profiles randomly picked from the aforementioned dataset.

### 2.4.3. Scenario 3

To show the impact of Level 2 residential charging on the distribution transformer's life, in this scenario, all the EVs are considered to be charging at Level 2. This is especially the case with single-household dwellings. In this scenario as well all EVs have different charging profiles.

### 2.4.4. Scenario 4

In order to generate an extreme condition, in this scenario, a 40% EV penetration at Level 1 is considered such that it overlaps with the residential peak load demand hours. Due to overlapping, a lower penetration level at a lower charging level is considered as it represents a sufficiently extreme scenario. The EV charging profiles are selected from the aforementioned dataset such that their charging pattern overlaps with the residential peak load hours.

The EVs, while charging, operate at unity power factor (UPF), i.e., they absorb active power only. Figure 2 shows a comparison of the transformer loading with baseline load (without EV) and with additional EV charging at UPF during Scenarios 1 to 4, respectively. It can be observed that with additional EV charging, the load line has increased significantly from the baseline level. To quantify the impact of this increased loading on the transformer's life, in the next section, transformer aging and insulation life calculations are discussed.

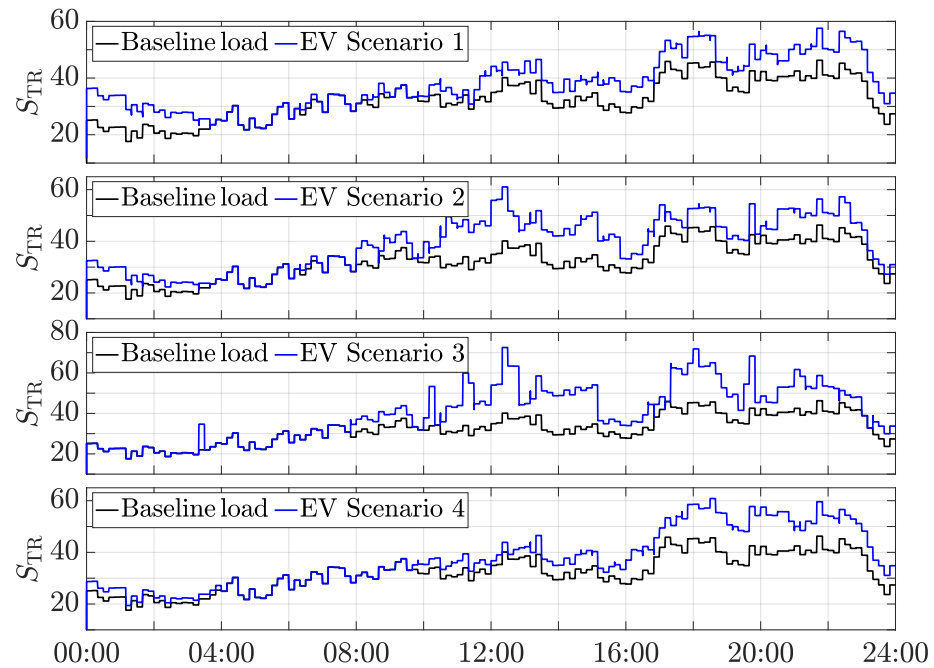


**Figure 2.** Transformer loading under different EV charging scenarios ( $S_{TR}$  in kVA).

### 3. Transformer Aging

According to the IEEE Standard C57.91-2011, winding insulation degradation is a dominant failure mechanism in oil-filled transformers [32]. The insulation aging is determined based on the winding hottest-spot temperature, formulated in Annex G of [32]. The heat balance equation is

$$Q_{GEN} = Q_{ABS} + Q_{LOST} \quad (1)$$

where  $Q_{GEN}$  and  $Q_{ABS}$  are the heat generated and absorbed by the source, respectively, and  $Q_{LOST}$  is the heat lost to the cooling medium [43]. The heat absorption equation is

$$Q_{ABS} = M \cdot C_P \cdot \Delta T \quad (2)$$

where  $M$  and  $C_P$  are the mass, and the specific heat of the material, respectively, and  $\Delta T$  is the time interval [43].

The heat generated by the hottest-spot ( $Q_{GEN,HS}$ ) is [32]

$$Q_{GEN,HS} = K^2 \left( P_{HS} K_{HS} + \frac{P_{EHS}}{K_{HS}} \right) \Delta t \quad (3)$$

where  $K$  is the ratio of the load during the interval  $\Delta t$  (in min.) to the rated load,  $P_{HS}$  and  $P_{EHS}$  are the winding  $i^2R$  and eddy losses in W, respectively, and  $K_{HS}$  is the temperature correction factor.

The heat lost at the hottest-spot is calculated as

$$Q_{LOST,HS} = \left( \frac{\theta_H^{t_1} - \theta_{WO}}{\theta_{H,R} - \theta_{WO,R}} \right)^{5/4} \left( \frac{\mu_{HS,R}}{\mu_{HS}^{t_1}} \right)^{1/4} (P_{HS} + P_{EHS}) \Delta t \quad (4)$$

where  $\theta_H^{t_1}$  and  $\theta_{H,R}$  are the winding hottest-spot temperatures at the prior time ( $t_1$ ) and at rated load in  $^{\circ}\text{C}$ , respectively;  $\theta_{WO}$  and  $\theta_{WO,R}$  are the temperatures of oil adjacent to the winding hot-spot, and at rated load in  $^{\circ}\text{C}$ , respectively;  $\mu_{HS,R}$  and  $\mu_{HS}^{t_1}$  are the viscosity

of fluid for hot-spot calculation at rated load and at the prior time ( $t_1$ ), in cP, respectively. From Equations (1) and (2)

$$\Delta T_{HS} = \frac{Q_{GEN,HS} - Q_{LOST,HS}}{M_W C_{P_W}} \quad (5)$$

where  $M_W C_{P_W}$  is the winding mass times specific heat in W-min/ $^{\circ}$ C. The recursive relation between winding hot-spot temperatures at successive time instants  $t_1$  and  $t_2 = t_1 + \Delta t$  is

$$\theta_H^{t_2} = \theta_H^{t_1} + \Delta T_{HS}. \quad (6)$$

Substituting Equation (5) in (6),

$$\theta_H^{t_2} = \frac{Q_{GEN,HS} - Q_{LOST,HS} + M_W C_{P_W} \theta_H^{t_1}}{M_W C_{P_W}} \quad (7)$$

where  $\theta_H^{t_2}$  is the winding hottest-spot temperature at the next instant of time. Using Equation (7), the transformer's aging is estimated by computing the aging accelerated factor given by

$$F_{AA} = \exp\left(\frac{15,000}{383} - \frac{15,000}{\theta_H^{t_2} + 273}\right), \quad (8)$$

where  $F_{AA}$  is equal to 1 at reference temperature,  $\theta_{H,ref}$ . In this study,  $\theta_{H,ref}$  is 110  $^{\circ}$ C as suggested in Annex I in [32]. Subsequently,  $F_{AA}$  is aggregated over the time period to calculate the equivalent aging factor

$$F_{EQA} = \frac{\sum_{n=1}^N F_{AA,n} \Delta t_n}{\sum_{n=1}^N \Delta t_n} \quad (9)$$

where  $\Delta t_n$  is time interval (in hours), and  $N$  is the total number of time intervals. The  $F_{EQA}$  is used to estimate transformer loss of life,  $LoL$ , which is the equivalent hours of insulation life consumed in the given time period, calculated from

$$\%LoL = \frac{F_{EQA} \times t \times 100}{L_{norm}} \quad (10)$$

where  $L_{norm}$  is the normal insulation life of the transformer, determined based on the standard values listed in [32].

Figure 3 shows the computed hottest-spot temperature and  $F_{AA}$  under baseline load and different EV charging scenarios discussed in Section 2. Table 1 shows  $F_{EQA}$  and  $LoL$  values. It is seen that increased EV penetration significantly impacts the transformer's life decreasing it by nearly 10, 14, 66, and 22 times the baseline load, in Scenario 1 to Scenario 4, respectively.

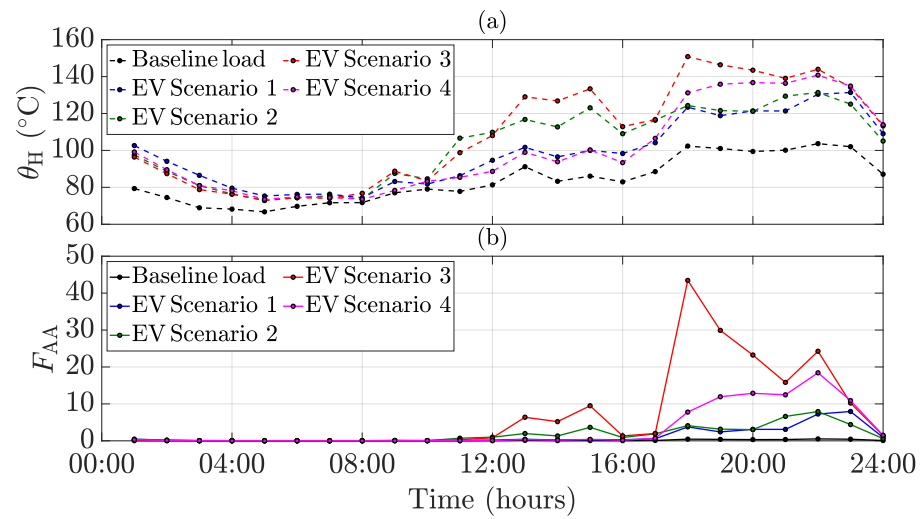


**Figure 3.** Transformer life indices without EV and with EV charging, (a) hottest-spot temperature,  $\theta_H$ ; (b) accelerated aging factor,  $F_{AA}$ .

**Table 1.** Transformer's  $F_{EQA}$  and  $LoL$  without EV and with EV charging.

Parameter	Baseline	Scenario 1	Scenario 2	Scenario 3	Scenario 4
$F_{EQA}$	0.137	1.35	1.91	9.12	2.99
$LoL$	3.29	32.45	45.78	218.84	71.69

#### 4. Proposed Method

The proposed solution is discussed in two parts. First, this paper proposes an EV-based reactive power compensation strategy for transformer overloading mitigation. And thereafter, a low-bandwidth centralized recursive controller is proposed to control the EV's onboard charger's reactive power supply.

##### 4.1. Reactive Power Compensation to Improve Transformer Life

From the discussion made in Section 3, specifically from the equations of heat generated at the hottest-spot, Equation (3) and the hottest-spot temperature Equation (7), it can be concluded that the transformer's insulation life can be extended by reducing the overall losses in the transformer. It can be observed that the transformer  $i^2R$  and eddy-current losses are a function of the winding currents. If the transformer real and reactive powers are denoted by  $P_{TR}$  and  $Q_{TR}$  respectively, the current flowing in the transformer is

$$I_{TR} = \frac{S_{TR}}{V_{TR}} = \frac{\sqrt{P_{TR}^2 + Q_{TR}^2}}{V_{TR}} \quad (11)$$

where  $S_{TR}$  is the apparent power, and  $V_{TR}$  is the rms voltage on the secondary side of the transformer. In the proposed method, a component of the residential reactive power demand ( $Q_R$ ) is supplied locally by the EV ( $Q_{EV}^i$ ) during charging as illustrated in Figure 4. Consequently, the overall reactive power flowing through the transformer ( $Q_{TR}$ ) is decreased. From Equation (11), it is evident that this reduces  $I_{TR}$  magnitude and thus decreases the overall losses in the transformer.

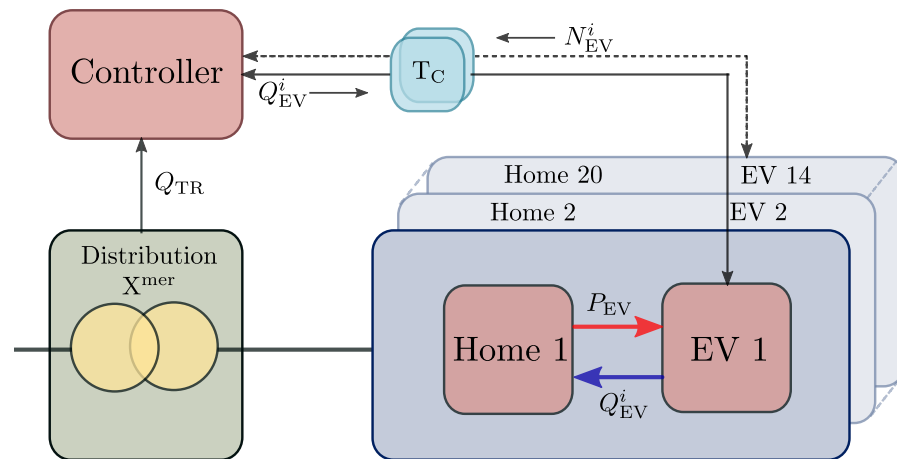


Figure 4. Entire system’s block diagram.

#### 4.2. Proposed Controller

The proposed controller is based on the aforementioned idea. It is a secondary-level recursive controller that generates the reference reactive power set points for the primary controllers of individual EVs connected to the distribution system. These references are then communicated to the EV chargers with communication delay,  $T_c$  (see Figure 4). The inputs to the controller are the transformer’s total reactive power and the number of EVs online. The reactive power compensation capability of active-front end rectifiers in onboard EV chargers using the DC-link capacitor has been shown in literature and is therefore not discussed in this paper [44–46].

##### 4.2.1. Problem Definition and Formulation

In the proposed approach, the EVs contribute to reactive power support without compromising their rate of charging (i.e., real power). The degree to which an EV can contribute is determined by the over-current limitations of the charger and residential ac outlets. Assume that the number of EVs online at any given time is  $N_{EV}$ , and the active power consumed and reactive power supplied by an EV is  $P_{EV}^i$  and  $Q_{EV}^i$ , respectively, where,  $i = 1, 2, \dots, N_{EV}$ . Thus,  $P_{EV}^i$  depends on the charging level and remains constant and the charger supplies  $Q_{EV}^i$  based on the reference set points computed by the controller. The increase in overall  $S_{EV}^i$  must not violate the maximum current limit of either the EV charger or the residential 120 V ac outlet [47]. Thus,

$$I_{EV}^i \leq I_{EV,max}^i \tag{12}$$

where,

$$I_{EV,max}^i = \min(I_{CH,max}^i, I_{REC,max}^i), \tag{13}$$

where  $I_{CH,max}$  is the maximum current limit of the EV charger, and  $I_{REC,max}$  is the maximum current limit of the ac outlet. The constraint in Equation (12) may be written as

$$Q_{EV}^i \leq Q_{EV,max}^i \quad i = 1, 2, \dots, N_{EV} \tag{14}$$

$$Q_{EV,max}^i = \sqrt{(S_{EV,max}^i)^2 - (P_{EV}^i)^2} = \frac{\sqrt{1 - (PF_{EV,min}^i)^2}}{PF_{EV,min}^i} P_{EV}^i \tag{15}$$

where  $S_{EV,max}^i$  is the maximum apparent power equal to  $I_{EV,max}^i V_{EV}$ , and  $PF_{EV,min}^i$  is the minimum power factor of the  $i^{th}$  EV equal to  $P_{EV}^i / S_{EV,max}^i$ . The problem formulation is to minimize  $Q_{TR}$  subject to the constraints in Equation (14).

### 4.2.2. Controller Structure and Design

The overall block diagram of the distribution system, including the transformer, the proposed controller, the communication system, and the EVs, is shown in Figure 4. The controller operates recursively and has a time step of  $T_s$ . It receives  $Q_{TR}$  and  $N_{EV}$  at intervals given by  $nT_s$ , where  $n \in \mathbb{Z}$ , and generates  $Q_{EV}^i$  for each EV.

The transformer’s reactive power  $Q_{TR}$  is given as

$$Q_{TR}[n] = Q_R[n] - Q_{EV}^{tot*}[n] \tag{16}$$

where  $Q_R$  is the total residential reactive power demand, and  $Q_{EV}^{tot*}$  is the aggregate reactive power compensation observed at the transformer location. From Figure 5  $Q_{EV}^{tot}$  is aggregate reactive power supplied by all the connected EVs.

$$Q_{EV}^{tot}[n] = \sum_{i=1}^{N_{EV}[n]} Q_{EV}^i[n] \tag{17}$$

where  $Q_{EV}^i$  denotes the share of the  $i$ th EV.

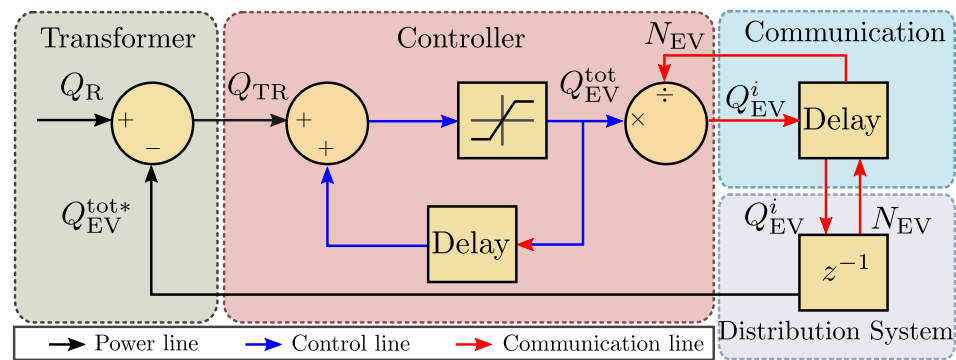


Figure 5. Simplified system and controller model.

The centralized controller receives the distribution transformer’s  $Q_{TR}$  value in real-time. It is conveniently located at the transformer site and measures the flow of reactive power at that interconnection. The controller’s objective is to minimize  $Q_{TR}$ . This occurs when  $Q_{EV}^{tot}$  tracks  $Q_R$ . Therefore, the overall control problem can be framed as a tracking problem where  $Q_{TR}$  represents the tracking error. The system diagram with the controller is shown in Figure 5. The overall EV system response is represented by a unit delay block. This mainly represents the delay of the distribution level communication infrastructure, which is typically much larger compared to the EV charger’s  $P$ ,  $Q$  control loops.

The controller shown in Figure 5 is essentially an integrator implemented in the discrete-time domain. The controller’s output is passed through a limiter whose limits are set as per the constraints in Equation (14). Therefore, the controller’s function can be expressed by

$$Q_{EV}^{tot}[n + 1] = \min(Q_{EV}^{tot*}[n] + Q_{TR}[n], Q_{EV,max}^{tot}) \tag{18}$$

where  $Q_{EV,max}^{tot}$  is the limit for  $Q_{EV}^{tot}$ .

The controller sends the  $Q_{EV}^i$  command to the individual EVs. Therefore, it is necessary to calculate  $Q_{EV}^i$ , where  $i = 1, 2, \dots, N_{EV}$  from  $Q_{EV}^{tot}$ . If all EVs are at the same charging level and equally incentivized, the total compensation,  $Q_{EV}^{tot}$  in Equation (17), can be expressed as

$$Q_{EV}^{tot}[n] = N_{EV}[n] Q_{EV}^i[n]. \tag{19}$$

Rearranging Equation (19), we get

$$Q_{EV}^i[n] = \frac{Q_{EV}^{tot}[n]}{N_{EV}[n]}. \tag{20}$$

Rewriting Equation (18) in terms of reactive power by individual EVs,  $Q_{EV}^i$ , when they are equally incentivized, we get

$$Q_{EV}^i[n+1] = \min\left(\frac{Q_{EV}^i[n]N_{EV}[n]+Q_{TR}[n]}{N_{EV}[n+1]}, Q_{EV,max}^i\right) \tag{21}$$

where  $Q_{EV,max}^i$  is obtained from constraints in Equation (14).

In a more general case where both Level 1 and Level 2 charging is present,  $Q_{EV}^{tot}$  becomes

$$Q_{EV}^{tot}[n] = \sum_{i=1}^{N_{EV,L1}[n]} Q_{EV,L1}^i[n] + \sum_{i=1}^{N_{EV,L2}[n]} Q_{EV,L2}^i[n] \tag{22}$$

where  $N_{EV,L1}[n]$  and  $N_{EV,L2}[n]$  are the number of EVs charging at Level 1 and Level 2, respectively, and they satisfy  $N_{EV}[n] = N_{EV,L1}[n] + N_{EV,L2}[n]$ . The reactive power limits for these charging levels are different and given by  $\pm Q_{EV,L1,max}^i$  and  $\pm Q_{EV,L2,max}^i$ , respectively. In this case, the maximum reactive power that can be supplied by EVs charging at Level 1 is  $N_{EV,L1}[n]Q_{EV,L1,max}^i$ , and at Level 2 is  $N_{EV,L2}[n]Q_{EV,L2,max}^i$ . Thus, the proportional share by each EV charging type is  $\frac{N_{EV,La}[n]Q_{EV,La,max}^i}{N_{EV,L2}[n]Q_{EV,L2,max}^i + N_{EV,L1}[n]Q_{EV,L1,max}^i}$ , where,  $a$  indicates the charging level,  $a = 1$  for Level 1, and  $a = 2$ , for Level 2. Therefore,  $Q_{EV}^{tot}$  is divided proportionally between EVs of each type to arrive at

$$Q_{EV}^i[n] = \begin{cases} \frac{Q_{EV}^{tot}[n]}{N_{EV,L1}[n]} \left( \frac{N_{EV,L1}[n] Q_{EV,L1,max}^i}{N_{EV,L2}[n] Q_{EV,L2,max}^i + N_{EV,L1}[n] Q_{EV,L1,max}^i} \right), & \text{Level 1} \\ \frac{Q_{EV}^{tot}[n]}{N_{EV,L2}[n]} \left( \frac{N_{EV,L2}[n] Q_{EV,L2,max}^i}{N_{EV,L2}[n] Q_{EV,L2,max}^i + N_{EV,L1}[n] Q_{EV,L1,max}^i} \right), & \text{Level 2.} \end{cases} \tag{23}$$

### 4.3. Stability Analysis under Communication Delays

From the high-level block diagram of the overall system shown in Figure 4, and the discussion in Section 4.2, it is established that a real-time  $Q_{TR}$  value of the transformer is available to the controller and it computes  $Q_{EV}^i$  set points and communicates them to the corresponding individual EVs. Now, there are several different communication protocols that are in use today [48]. The proposed controller implementation is agnostic to the exact communication protocol and thus can be used under the various protocols. This section discusses the controller stability under these communication delays.

In Figure 6 of the proposed recursive controller, the communication delay is denoted by  $T_C$ , and the controller recursive feedback time is denoted by  $T_F$ , which in  $z$ -domain are represented as  $z^{-C}$  and  $z^{-F}$  respectively, where  $C, F \in \mathbb{N}$ . The transfer function  $\frac{Q_{EV}^{tot}(z)}{Q_R(z)}$  for the generalized system is derived below. From Figure 6

$$Q_{TR}(z) + z^{-F}Q_{EV}^{ctr}(z) = Q_{EV}^{ctr}(z) \tag{24}$$

where, in addition to the previous definitions,  $Q_{EV}^{ctr}(z)$  is the controller output. By rearranging (24) we get,

$$Q_{TR}(z) = Q_{EV}^{ctr}(z)(1 - z^{-F}). \tag{25}$$

Again from Figure 6,

$$Q_{EV}^{tot}(z) = z^{-C}Q_{EV}^{ctr}(z). \tag{26}$$

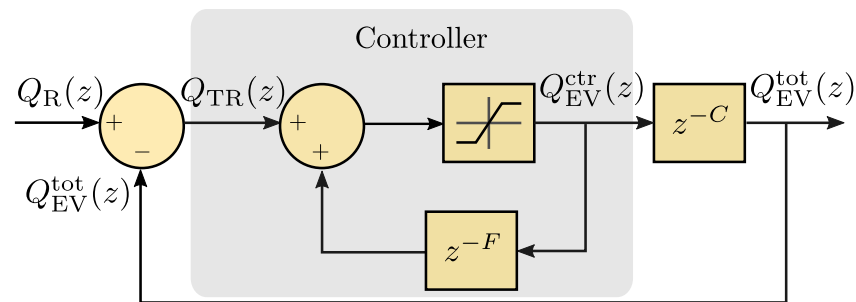


Figure 6. Simplified system and controller model for stability analysis.

By rearranging and substituting the above equations we get,

$$\frac{Q_{EV}^{tot}(z)}{Q_R(z)} = \frac{z^{-C}}{z^{-C} - z^{-F} + 1}. \quad (27)$$

Therefore, the final transfer function  $H(z)$  is given by

$$H(z) = \frac{Q_{EV}^{tot}(z)}{Q_R(z)} = \frac{1}{z^C - z^{C-F} + 1}, \quad C, F \in \mathbb{N}. \quad (28)$$

To determine the conditions under which the proposed controller is stable, stability criterion from [49] can be applied to the characteristic polynomial  $D(z)$ , of the transfer function  $H(z)$  in Equation (28). If the characteristic polynomial of the system is given by

$$D(z) = a_0 + a_1z^1 + a_2z^2 + \dots + a_{n-1}z^{n-1} + a_nz^n \quad (29)$$

then one necessary condition for its stability is

$$|a_0| < a_n, \quad a_n > 0 \quad (30)$$

where  $a_n$  is the co-efficient of the largest power term  $z^n$ , and  $a_0$  is the constant term in  $D(z)$ . From Equation (28),  $D(z) = z^C - z^{C-F} + 1$ . For  $C, F \in \mathbb{N}$ , 3 possible cases exists, case 1:  $C > F$ , case 2:  $F > C$ , and case 3:  $F = C$ . Rewriting  $D(z)$  in increasing order of positive powers of  $z$  for the two first cases we get,

$$D(z) = \begin{cases} 1 - z^{C-F} + z^C, & C > F \\ -1 + z^{F-C} + z^F, & F > C \end{cases}, \quad C, F \in \mathbb{N}. \quad (31)$$

It can be seen that for both these cases,  $|a_0| = 1; a_n = 1$  therefore, the condition in Equation (30) is not satisfied. However, for case 3, when  $F = C$ ,  $D(z) = z^C$ . Thus,  $a_0 = 0; a_n = 1$  and  $|a_0| < |a_n|$  satisfy. Moreover, all the roots of  $D(z)$  are located at the origin, i.e., inside the unit circle, which indicates its stability. Therefore, in this case, the transfer function,  $H(z)$  becomes

$$H(z) = \frac{Q_{EV}^{tot}(z)}{Q_R(z)} = z^{-C}. \quad (32)$$

From Equation (32),  $H(z)$  has a single pole at  $z = 0$ , which lies within the unit circle in the complex plane. Therefore, the closed-loop system in Figure 6 is stable. Intuitively, Equation (32) implies that  $Q_{EV}^{tot}$  tracks the input  $Q_R$  with a delay of  $C$  time steps.

## 5. Results and Discussion

In this section, numerical simulation results, obtained using Matlab/Simulink, pertaining to the study system with the proposed controller for EV charging are presented and discussed.

### 5.1. Description of Simulation System

The proposed controller is implemented on the study system of Figure 1. The controller receives the locally-measured transformer reactive power  $Q_{TR}$  and the number of online EVs  $N_{EV}$ , and it computes  $Q_{EV}^i$  and communicates it to the corresponding individual EVs. The communication between the controller and the EV is two-way. When plugged in, the EV sends an “On-Plug” status signal to the controller [50]. In the simulation, this corresponds to the variable  $N_{EV,La}^i$  for  $i$ th EV, where  $a$  is 1 for Level 1, and 2 for Level 2 charging. Similarly, the controller sends back the  $Q_{EV}^{i,a}$  values to the individual EVs online. The communication latency is denoted by  $T_C$ , which is assumed to be 5 s in this study. The limit for  $I_{EV,max}^i$  in Equation (12) is considered at 120% of the charger’s rated current capacity. Thus, from Equation (14), at Level 1,  $Q_{EV,max}^i$  is 1.44 kVAR, and at Level 2,  $Q_{EV,max}^i$  is 4.95 kVAR.

### 5.2. Scenario 1: EV Charging at Level 1

In this scenario, all EVs are charging at Level 1. Figure 7 shows the simulation results. Figure 7a shows the number of EVs present where  $N_{EV,tot}$  is the total number of EVs online (charging at Level 1 + Level 2),  $N_{EV,L1}$  and  $N_{EV,L2}$  values represent the total EVs online at Level 1 and Level 2, respectively. In this scenario,  $N_{EV,L2} = 0$ . Figure 7b shows a comparison of the transformer kVA for baseline load, aggregate load in Scenario 1, and aggregate load with the proposed compensation technique.

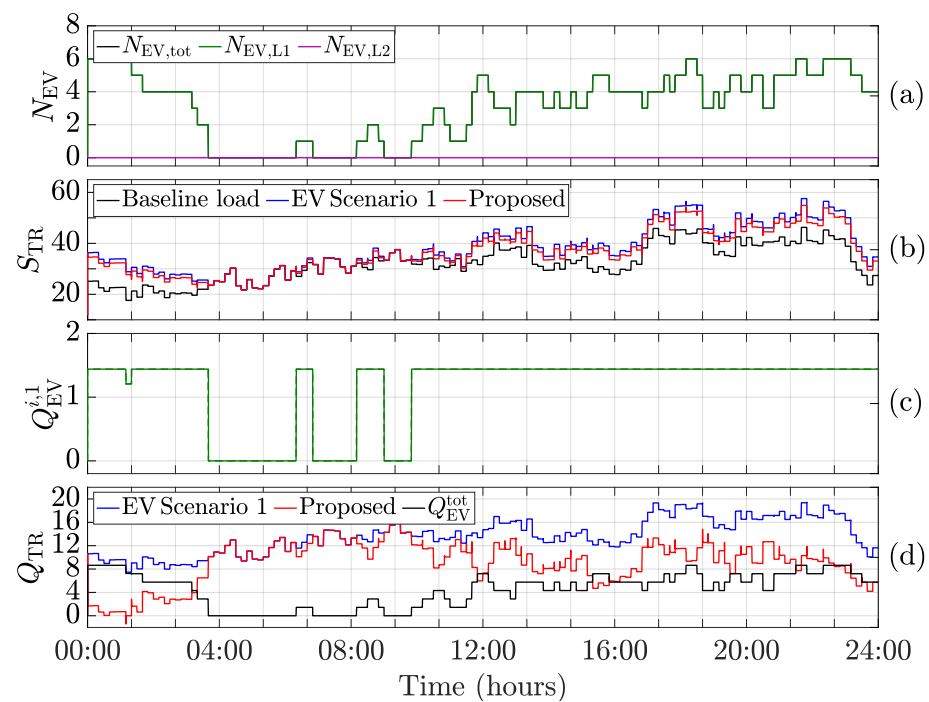


**Figure 7.** Scenario 1: EV charging at Level 1, (a) number of EVs present; (b) transformer apparent power in kVA; (c)  $Q$  supplied by an online EV at Level 1 in kVAR; (d) transformer reactive power in kVAR.

Figure 7c shows reactive power compensated by a single EV. Finally, Figure 7d shows  $Q_{TR}$  magnitude without and with the proposed method, and the aggregate compensation,  $Q_{EV}^{tot}$  by online EVs.

Figure 7d shows the total transformer reactive power  $Q_{TR}$  measured at the transformer. Equation (16) shows the reactive power balance at that point. However, neither  $Q_R$  nor  $Q_{EV}^{tot*}$  can be measured directly. Therefore, in this figure  $Q_{TR}$  along with the controller output  $Q_{EV}^{tot}$  is shown. Figure 7b,d show that the proposed controller reduces the aggregate loading on the transformer. To quantify this reduction in terms of transformer aging, the

transformer's winding hottest-spot temperature is calculated and compared as shown in Figure 8. Figure 8a shows that for baseline load,  $\theta_H$  is always less than  $\theta_{H,ref}$  (110 °C). Hence, the  $F_{AA}$  is always less than 1 in Figure 8b. However, an increase in the aggregate load under Scenario 1 results in increased transformer losses, and thus its winding temperature. Therefore, it can be observed that  $\theta_H$  reaches well above  $\theta_{H,ref}$ , and consequently, there is a significant increase in  $F_{AA}$ . Specifically, between 21:00 and 24:00 h,  $\theta_H$  nearly reaches 130 °C, resulting in  $F_{AA}$  equal to 8. With the proposed reactive power compensation method,  $\theta_H$  decreases which results in  $F_{AA}$  decreasing by nearly 50%. Furthermore, the equivalent aging factor,  $F_{EQA}$  is calculated using Equation (9), and  $LoL$  is calculated by multiplying  $F_{EQA}$  with  $t$ . The results are summarized in Table 2. Before compensation, the transformer's  $LoL$  is nearly 10 times the baseline value, but with the proposed controller, it decreases significantly. It is concluded that the proposed solution compensates for the increased loading during EV charging Scenario 1 and, as a result, the transformer's aging is reduced by almost 44% in comparison to the case without the proposed method.

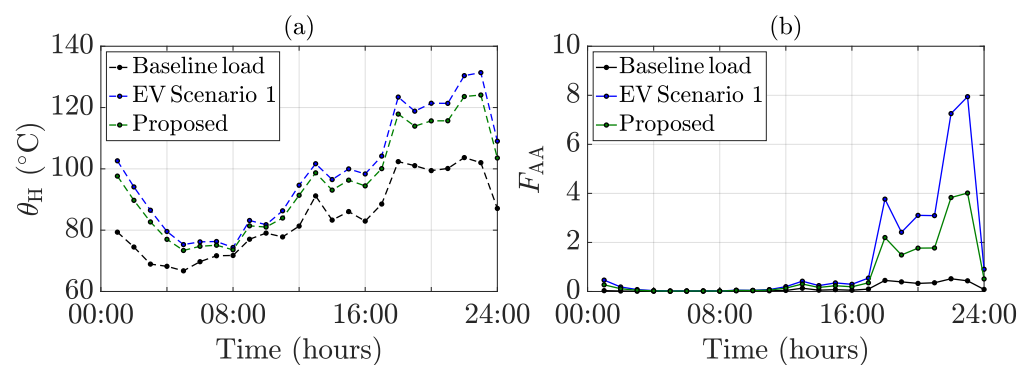


**Figure 8.** Transformer life indices in scenario 1, (a) hottest-spot temperature,  $\theta_H$ ; (b) accelerated aging factor,  $F_{AA}$ .

**Table 2.**  $F_{EQA}$  and  $LoL$  in scenario 1.

System	$F_{EQA}$	$LoL$ (h)
Baseline load	0.137	3.29
EV Scenario 1	1.35	32.45
Proposed method	0.757	18.18

The increased power demand due to EV charging is likely to cause under-voltage conditions in the secondary distribution system. Since maintaining an appropriate voltage level is important to ensure power quality, this paper also evaluates the impact of EV charging on the load bus voltages and discusses the efficacy of the proposed method in improving the bus voltage profiles. Figure 9 shows the voltage profile under Scenario 1 with and without the proposed controller of a few load buses. The improvement achieved by the proposed method is visible. To show the deviation in voltage under Scenario 1 from the baseline system voltages, the root mean square deviation is calculated as

$$V_{RMSD} = \sqrt{\frac{\sum_{i=1}^M (V_{pk}(i) - V_{base,pk}(i))^2}{M}} \quad (33)$$

where  $V_{RMSD}$  is the root mean square deviation in voltage over 24 h;  $V_{base,pk}(i)$  and  $V_{pk}(i)$  are the peak voltages at  $i$ th instant for the baseline system and the comparative system, respectively;  $M$  = number of data points. Table 3 shows the calculated  $V_{RMSD}$  in phase voltages  $L_1 - N$ ,  $L_2 - N$  and line voltage  $L_1 - L_2$  under Scenario 1 with and without proposed method from the baseline load voltages for all the 20 load buses. It can be

concluded from Figure 9 and Table 3 that with the proposed method, the voltage deviations as well as the voltage excursions outside the acceptable range have significantly reduced.

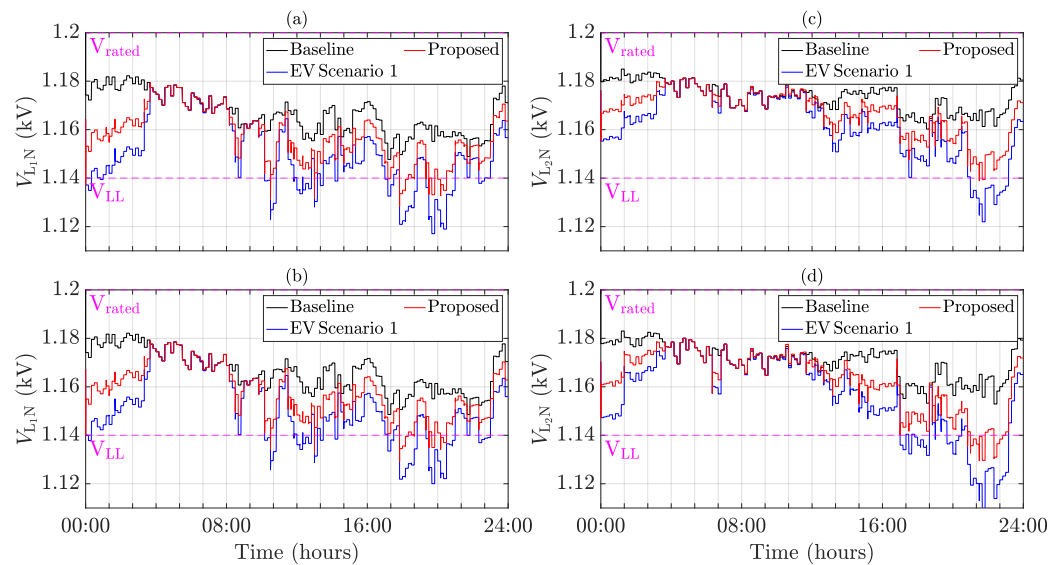


**Figure 9.** Phase voltages in scenario 1, (a) at bus 10 with EV charging between phase  $L_1 - N$ ; (b) at bus 15 with no EV present at it; (c) at bus 8 with EV charging between phase  $L_2 - N$ ; (d) at bus 13 with EV charging between phase  $L_2 - N$ .

**Table 3.** Root mean square deviation in voltages in scenario 1 with and without the proposed method.

Phase/Line	$L_1 - N$	$L_1 - N$	$L_2 - N$	$L_2 - N$	$L_1 - L_2$	$L_1 - L_2$
Bus No.	w/o Controller	with Controller	w/o Controller	with Controller	w/o Controller	with Controller
Bus 1	2.15	1.16	0.44	0.29	1.75	0.9
Bus 2	1.98	1.06	0.38	0.27	1.65	0.8
Bus 3	2.18	1.19	0.44	0.29	1.77	0.92
Bus 4	2.05	1.1	0.41	0.28	1.69	0.84
Bus 5	0.44	0.29	2.12	1.14	1.72	0.88
Bus 6	0.45	0.29	2.15	1.16	1.74	0.9
Bus 7	0.44	0.29	2.13	1.14	1.73	0.88
Bus 8	0.48	0.3	2.24	1.22	1.8	0.94
Bus 9	2.86	1.64	0.72	0.38	2.19	1.31
Bus 10	2.87	1.64	0.72	0.38	2.19	1.31
Bus 11	2.82	1.61	0.7	0.37	2.16	1.28
Bus 12	0.58	0.34	2.53	1.41	1.99	1.11
Bus 13	0.64	0.36	2.7	1.52	2.1	1.21
Bus 14	0.28	0.09	0.34	0.09	0.6	0.16
Bus 15	2.72	1.54	0.66	0.36	2.1	1.23
Bus 16	0.57	0.33	2.49	1.38	1.96	1.09
Bus 17	0.29	0.09	0.3	0.08	0.58	0.16
Bus 18	0.29	0.09	0.3	0.08	0.58	0.16
Bus 19	0.29	0.09	0.3	0.08	0.58	0.16
Bus 20	0.57	0.33	2.49	1.38	1.96	1.09

### 5.3. Scenario 2: Combined Level 1 and Level 2 EV Charging

To understand the impact of Level 2 charging on the current distribution system infrastructure, in this scenario some EVs are considered to be charging at Level 2. Figure 10a shows the number of online EVs at any given time. It can be observed from Figure 10b that with only partial Level 2 charging penetration, the transformer load peak,  $S_{TR}$ , exceeds 60 kVA. The reactive power compensation by EVs charging at Level 1,  $Q_{EV}^{i,1}$ , and at Level 2,

$Q_{EV}^{i,2}$ , are shown in Figure 10c,d, respectively. Depending on the charging level, number of EVs online, and the total capacity ( $Q_{EV,L1,max}^i, Q_{EV,L2,max}^i$ ) of the EVs at any given time, Equation (23) is used to calculate the  $Q_{EV}^{i,1}$  and  $Q_{EV}^{i,2}$  values. Figure 10e, shows that with the proposed method the transformer reactive power ( $Q_{TR}$ ) decreases.

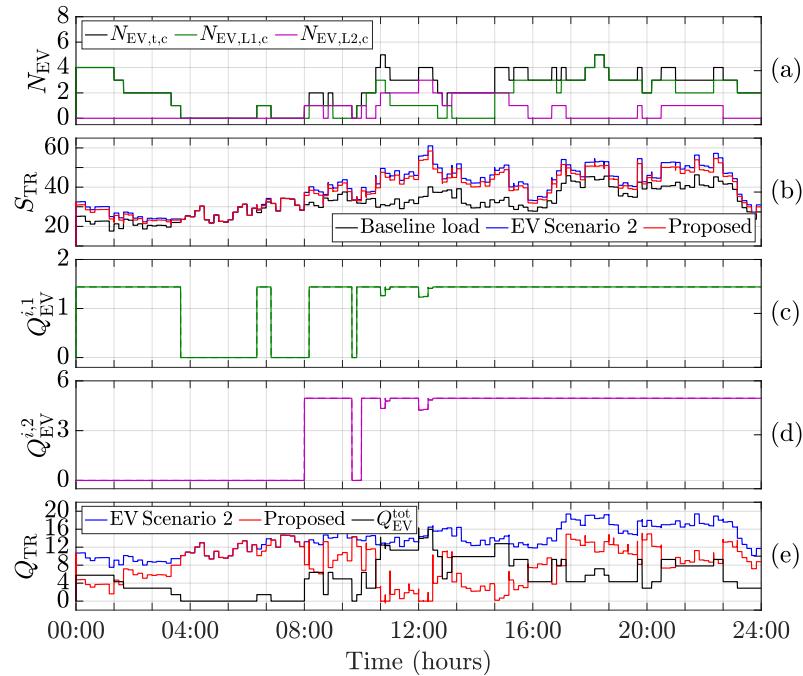


**Figure 10.** Scenario 2: combined Level 1 and Level 2, (a) number of EVs present; (b) transformer apparent power in kVA; (c)  $Q$  supplied by an online EV at Level 1 in kVAR; (d)  $Q$  supplied by an online EV at Level 2 in kVAR; (e) transformer reactive power in kVA.

The transformer life indices are presented in Figure 11 and Table 4. The increased loading due to the addition of Level 2 charging results in  $\theta_H$  exceeding  $\theta_{H,ref}$  more frequently and for an extended duration compared to Scenario 1. A similar trend can be observed in  $F_{AA}$  plot, and thus  $F_{EQA}$  values. This is also reflected in the increased transformer’s  $LoL$  of 45.79 h in Scenario 2 against 32.45 h in Scenario 1. With the proposed method,  $\theta_H$  and  $F_{AA}$  decrease. The  $F_{EQA}$  decreases by nearly 43% compared to  $F_{EQA}$  without compensation. The transformer’s  $LoL$  decreases from 45.79 h to 25.92 h with the proposed method which is nearly a 43% decrease in the transformer aging.

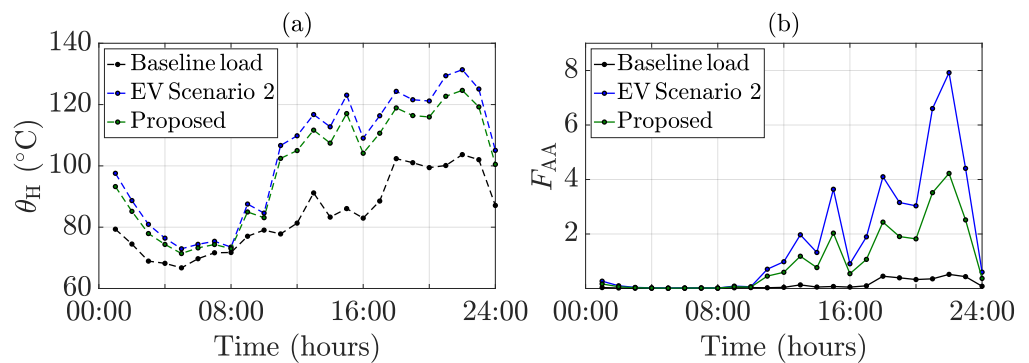


**Figure 11.** Transformer life indices in scenario 2, (a) hottest-spot temperature,  $\theta_H$ ; (b) accelerated aging factor,  $F_{AA}$ .

**Table 4.**  $F_{EQA}$  and  $LoL$  in scenario 2.

System	$F_{EQA}$	$LoL$ (h)
Baseline load	0.137	3.29
EV Scenario 2	1.91	45.79
Proposed method	1.08	25.92

Further, an increase in power demand due to Level 2 charging results in increased voltage drops at the corresponding buses. It can be observed from Table 5 that with the proposed method voltage deviations have reduced.

**Table 5.** Root mean square deviation in voltages in scenario 2 with and without the proposed method.

Phase/Line	$L_1 - N$	$L_1 - N$	$L_2 - N$	$L_2 - N$	$L_1 - L_2$	$L_1 - L_2$
Bus No.	w/o Controller	with Controller	w/o Controller	with Controller	w/o Controller	with Controller
Bus 1	1.6	0.88	0.74	0.35	1.84	0.94
Bus 2	1.5	0.83	0.86	0.46	1.97	1.06
Bus 3	1.41	0.75	0.8	0.38	1.76	0.86
Bus 4	1.57	0.86	0.76	0.36	1.81	0.92
Bus 5	1.5	0.83	1.04	0.58	2.4	1.33
Bus 6	1.35	0.76	1.19	0.69	2.46	1.39
Bus 7	1.42	0.83	1.25	0.74	2.59	1.53
Bus 8	1.28	0.7	1.12	0.62	2.31	1.26
Bus 9	1.74	0.99	1.01	0.56	2.07	1.17
Bus 10	1.91	1.1	0.97	0.52	2.11	1.21
Bus 11	1.77	1.01	0.97	0.54	2.1	1.21
Bus 12	1.16	0.65	1.71	1.01	2.59	1.52
Bus 13	1.19	0.66	1.49	0.86	2.48	1.41
Bus 14	0.47	0.11	0.44	0.13	0.91	0.23
Bus 15	1.75	0.99	0.94	0.51	2.04	1.14
Bus 16	1.19	0.66	1.49	0.86	2.48	1.41
Bus 17	0.39	0.09	0.34	0.11	0.73	0.2
Bus 18	0.39	0.09	0.34	0.11	0.73	0.2
Bus 19	0.39	0.09	0.34	0.11	0.73	0.2
Bus 20	1.19	0.66	1.49	0.86	2.48	1.41

#### 5.4. Scenario 3: EV Charging at Level 2

This scenario is representative of a near-future scenario where the majority of EVs will have Level 2 on-board chargers. Figure 12 shows the impact of EV charging on transformer loading in Scenario 3, and the effectiveness of the proposed method in mitigating it. With only Level 2 charging, the transformer loading is severely impacted with  $S_{TR}$  increasing up to 75 kVA. With the proposed method, this overloading is reduced to some extent. The compensation by EVs at Level 2 is shown in Figure 12c. It can be observed that during the time 11:00 to 15:00 h,  $Q_{TR}$  is mostly lower than that during 14:00 to 24:00 h. In addition, the number of EVs charging from 11:00 to 15:00 h are mostly either equal to or greater than the number of EVs charging during 14:00 to 24:00 h. Therefore, the individual reactive power supplied by each EV,  $Q_{EV}^i$ , is lower during the first interval resulting in  $Q_{TR}$  mostly becoming zero during the first interval, as can be observed from Figure 12d. This consequently reduces  $I_{TR}$  and thus the transformer losses.

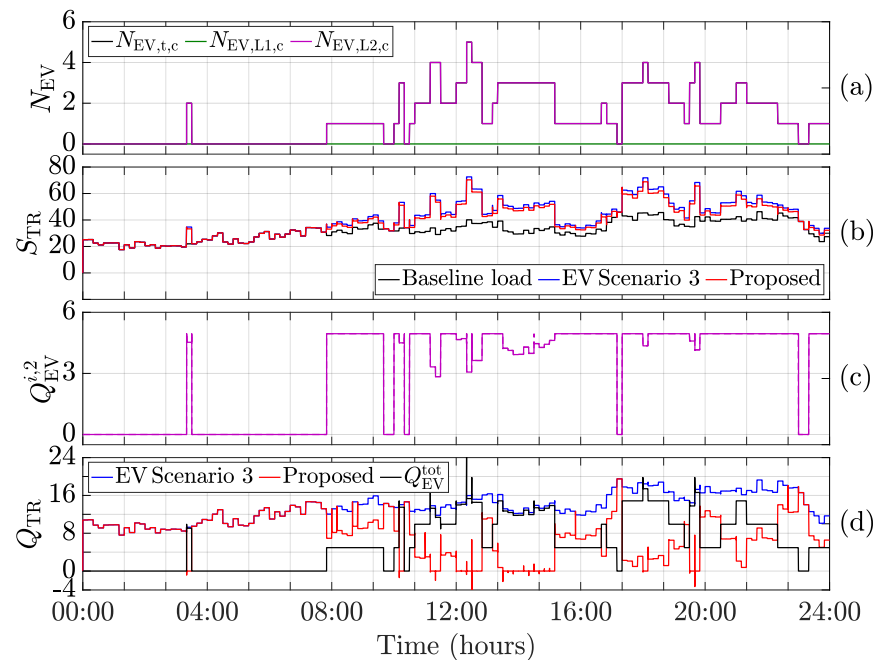


**Figure 12.** Scenario 3: EV charging at Level 2, (a) number of EVs present; (b) transformer apparent power in kVA; (c)  $Q$  supplied by an online EV at Level 2 in kVAr; (d) transformer reactive power in kVAr.

Parameters in Figure 13 quantify this reduction in terms of transformer life. Increased loading in Scenario 3 results in  $\theta_H$  increasing well above  $\theta_{H,ref}$  ( $110\text{ }^\circ\text{C}$ ) after 12:00 h, reaching as high as  $150\text{ }^\circ\text{C}$ . This causes a significant increase in  $F_{AA}$ . However, with the proposed solution, peak  $F_{AA}$  decreases by nearly 50%. Table 6 shows the  $F_{EQA}$  and transformer  $LoL$  in Scenario 3. With the proposed method the equivalent aging factor decreases by almost 48%, which leads to a corresponding reduction in transformer  $LoL$ . From the above discussion it can be concluded that in Scenario 3, which represents a likely worst case, the proposed method effectively improves the transformer life.

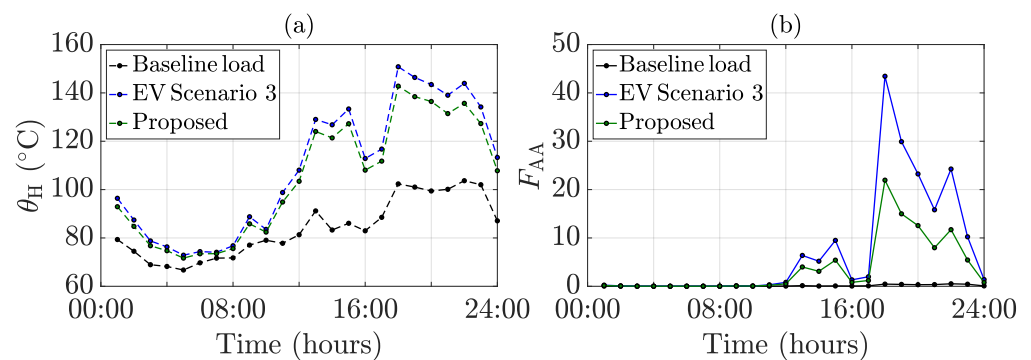


**Figure 13.** Transformer life indices in scenario 3, (a) hottest-spot temperature,  $\theta_H$ ; (b) accelerated aging factor,  $F_{AA}$ .

**Table 6.**  $F_{EQA}$  and  $LoL$  in scenario 3.

System	$F_{EQA}$	$LoL$ (h)
Baseline load	0.137	3.29
EV Scenario 3	9.12	218.84
Proposed method	4.74	113.71

Due to only Level 2 EV charging, the voltage profiles are severely impacted. However, with the proposed method these deviations are reduced to some extent. Table 7 shows the efficacy of the proposed method in reducing voltage deviations.

**Table 7.** Root mean square deviation in voltages in scenario 3 with and without the proposed method.

Phase/Line	L <sub>1</sub> – N	L <sub>1</sub> – N	L <sub>2</sub> – N	L <sub>2</sub> – N	L <sub>1</sub> – L <sub>2</sub>	L <sub>1</sub> – L <sub>2</sub>
Bus No.	w/o Controller	with Controller	w/o Controller	with Controller	w/o Controller	with Controller
Bus 1	1.28	0.7	1.28	0.7	2.55	1.4
Bus 2	1.32	0.75	1.32	0.75	2.65	1.5
Bus 3	1.19	0.63	1.19	0.63	2.38	1.25
Bus 4	1.21	0.65	1.21	0.65	2.42	1.29
Bus 5	1.54	0.91	1.54	0.91	3.08	1.83
Bus 6	1.52	0.89	1.52	0.89	3.04	1.77
Bus 7	1.55	0.93	1.55	0.93	3.1	1.86
Bus 8	1.44	0.83	1.44	0.83	2.89	1.66
Bus 9	1.56	0.98	1.56	0.98	3.12	1.96
Bus 10	1.62	1.03	1.62	1.03	3.24	2.07
Bus 11	1.51	0.93	1.51	0.93	3.02	1.86
Bus 12	1.93	1.29	1.93	1.29	3.86	2.57
Bus 13	1.9	1.27	1.9	1.27	3.81	2.53
Bus 14	0.62	0.17	0.62	0.17	1.23	0.33
Bus 15	1.51	0.93	1.51	0.93	3.02	1.85
Bus 16	1.81	1.18	1.81	1.18	3.63	2.36
Bus 17	0.48	0.11	0.48	0.11	0.97	0.22
Bus 18	0.48	0.11	0.48	0.11	0.97	0.22
Bus 19	0.48	0.11	0.48	0.11	0.97	0.22
Bus 20	1.81	1.18	1.81	1.18	3.63	2.36

#### 5.5. Scenario 4: EV Charging at Level 1 Extreme

The growing number of EVs may cause a scenario where a large number of EVs charge during peak load hours. Thus, in this scenario, 40% EV penetration at Level 1 is selected such that the EV charging profiles coincide with the peak load hours of the baseline load. The simulation results for this scenario are shown in Figure 14. As expected, between 18:00 and 23:00 h the transformer loading is always above 50 kVA, reaching as high as 60 kVA. With the proposed method, EVs are compensating at their limit,  $Q_{EV,L1,max}^i$  during this interval.

Figures 14b and 15 summarize the impact of Scenario 4 on the transformer loading and transformer's winding temperature respectively. Table 8 summarizes the calculated  $F_{EQA}$  and  $LoL$  values. It can be observed that  $F_{AA}$  value in Scenario 4 is significantly higher than Scenario 1 where 70% EV penetration at Level 1 is considered, and Scenario 2 where 70% EV penetration at combined Level 1 and 2 is considered. Thus indicating the severe impact of EV charging during peak load hours on the transformer life. With the proposed method,  $F_{EQA}$  decreases by nearly 50%, and the transformer's  $LoL$  reduces from 71.69 h to 35.83 h, i.e., transformer aging is reduced by nearly 50%. The proposed approach is also applicable if only Level 2 extreme or a mix of Level 1 and Level 2 extreme is considered. From the above discussion, it can be observed that the transformer life is impacted at a lower EV charging level. Thus, it can be concluded that with a higher EV charging (Level 2) overlapping with the peak load demand hours, the transformer life will further deteriorate, which then with the proposed controller will improve.

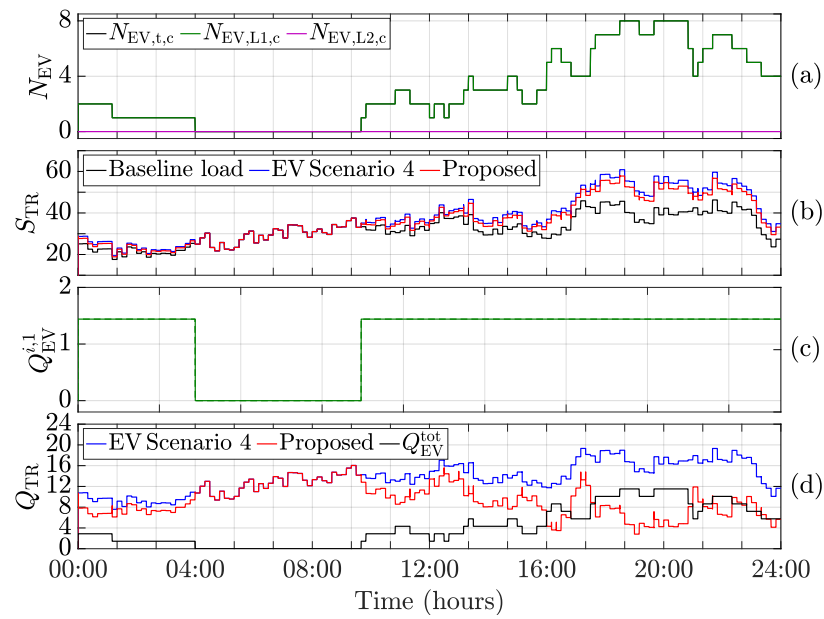


**Figure 14.** Scenario 4: EV charging overlaps with peak load, (a) number of EVs present; (b) transformer apparent power in kVA; (c) Q supplied by an online EV at Level 1 in kVar; (d) transformer reactive power in kVar.

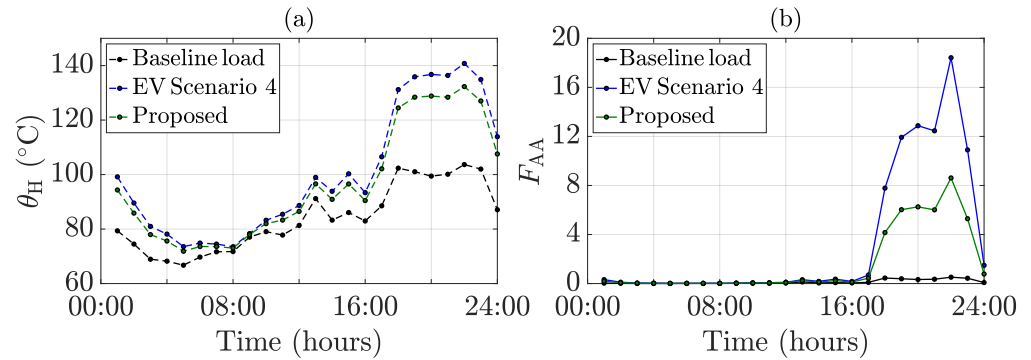


**Figure 15.** Transformer life indices in scenario 4, (a) hottest-spot temperature,  $\theta_H$ ; (b) accelerated aging factor,  $F_{AA}$ .

**Table 8.**  $F_{EQA}$  and  $LoL$  in scenario 4.

System	$F_{EQA}$	$LoL$ (h)
Baseline load	0.137	3.29
EV Scenario 4	2.99	71.69
Proposed method	1.49	35.83

Table 9 shows the deviation in voltage from the baseline load with and without the proposed method. It can be observed that  $V_{RMSD}$  decreases with the proposed method.

**Table 9.** Root mean square deviation in voltages in scenario 4 with and without the proposed method.

Phase/Line	L <sub>1</sub> – N	L <sub>1</sub> – N	L <sub>2</sub> – N	L <sub>2</sub> – N	L <sub>1</sub> – L <sub>2</sub>	L <sub>1</sub> – L <sub>2</sub>
Bus No.	w/o Controller	with Controller	w/o Controller	with Controller	w/o Controller	with Controller
Bus 1	2.2	1.14	0.42	0.3	1.81	0.87
Bus 2	2.36	1.25	0.47	0.32	1.92	0.96
Bus 3	2.19	1.14	0.41	0.3	1.81	0.87
Bus4	2.19	1.14	0.41	0.3	1.81	0.87
Bus 5	0.25	0.23	1.59	0.78	1.42	0.57
Bus 6	0.25	0.23	1.59	0.78	1.42	0.57
Bus 7	0.26	0.23	1.6	0.78	1.43	0.57
Bus 8	0.3	0.24	1.75	0.88	1.52	0.66
Bus 9	4.02	2.31	1.08	0.52	2.97	1.89
Bus 10	3.93	2.24	1.04	0.51	2.91	1.83
Bus 11	3.96	2.27	1.06	0.51	2.93	1.85
Bus 12	0.67	0.36	2.82	1.58	2.2	1.27
Bus 13	0.66	0.36	2.8	1.56	2.18	1.25
Bus 14	0.24	0.11	0.57	0.12	0.79	0.09
Bus 15	3.72	2.12	0.97	0.48	2.78	1.72
Bus 16	0.58	0.34	2.57	1.41	2.04	1.12
Bus 17	0.32	0.09	0.31	0.09	0.63	0.17
Bus 18	0.32	0.09	0.31	0.09	0.63	0.17
Bus 19	0.32	0.09	0.31	0.09	0.63	0.17
Bus 20	0.58	0.34	2.57	1.41	2.04	1.12

### 5.6. Annual Transformer Aging

The effect of seasonal variation in the residential electricity demand and the ambient temperature on the transformer life is not apparent in a 24 h simulation. Therefore, to study the impact of transformer overloading on its life considering seasonal variations in residential and EV charging load, the above simulations are performed for an entire year. The same dataset in [31] is used. The main objective is to calculate the annual equivalent aging factor, and annual transformer life consumed, *LoL*. Figure 16a,b, show the transformer's annual  $F_{EQA}$  and *LoL* (hours per year) for the considered scenarios. The results indicate that even with seasonal variation in load and ambient temperature, the proposed controller decreases the transformer aging by around 44%, 50%, and 52% in Scenario 1, 2, and 3 respectively when compared to the uncompensated case.

For the studies so far, 70% EV penetration is considered which is relatively high. To verify the efficacy of the proposed method at lower EV penetration, Scenario 5 with only 40% EV penetration at Level 1 is also considered (8 EVs in 20 houses). Table 10 shows the annual equivalent aging factor and the transformer insulation life consumption in one year in Scenario 5. It can be verified that the proposed technique is effective at lower EV penetrations as well. In Scenario 5, the transformer's *LoL* is almost 3.3 times the baseline load which with the proposed method decreases to nearly 2.3 times the baseline load, i.e., transformer aging is slowed by nearly 32%.

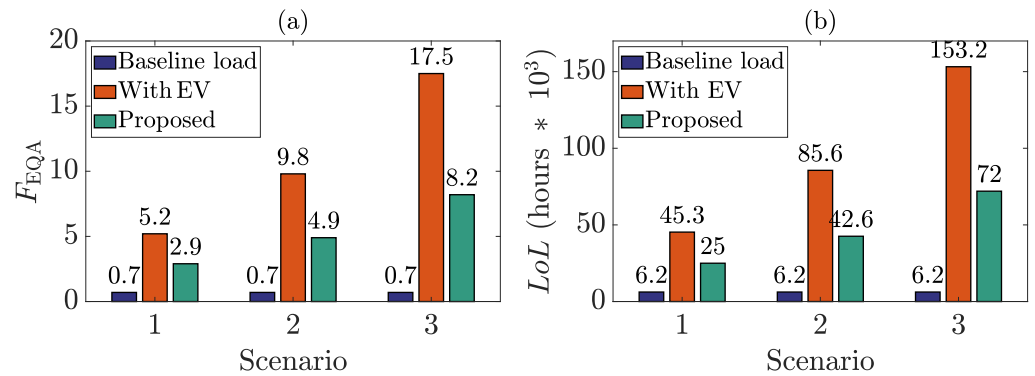


Figure 16. Transformer’s annual (a) equivalent aging factor,  $F_{EQA}$ ; and (b) loss of life,  $LoL$ .

Table 10. Annual  $F_{EQA}$  and  $LoL$  in scenario 5 (40 % EV penetration).

System	$F_{EQA}$	$LoL$ ( $\times 1000$ h)
Baseline load	0.71	6.18
EV Scenario 5	2.33	20.45
Proposed method	1.6	14

5.7. Analysis of Sensitivity to Communication Failures

A communication failure between the controller and the EV may happen in practice. Therefore, it is important to ensure that the proposed controller is robust to these communication failures. In this section, the controller’s robustness to three potential communication failures is evaluated.

5.7.1. Communication Failure Case 1

This case evaluates a failure scenario where the controller continues to receive an “On-Plug” signal from an EV that has disconnected. For this discussion, the communication link between EV-10 and the controller is assumed to have failed as shown in Figure 17. EV-10 stops charging at 10:50 h, but the correct communication isn’t restored until 11:10 h, thus for the controller EV-10 is online till 11:10 h.

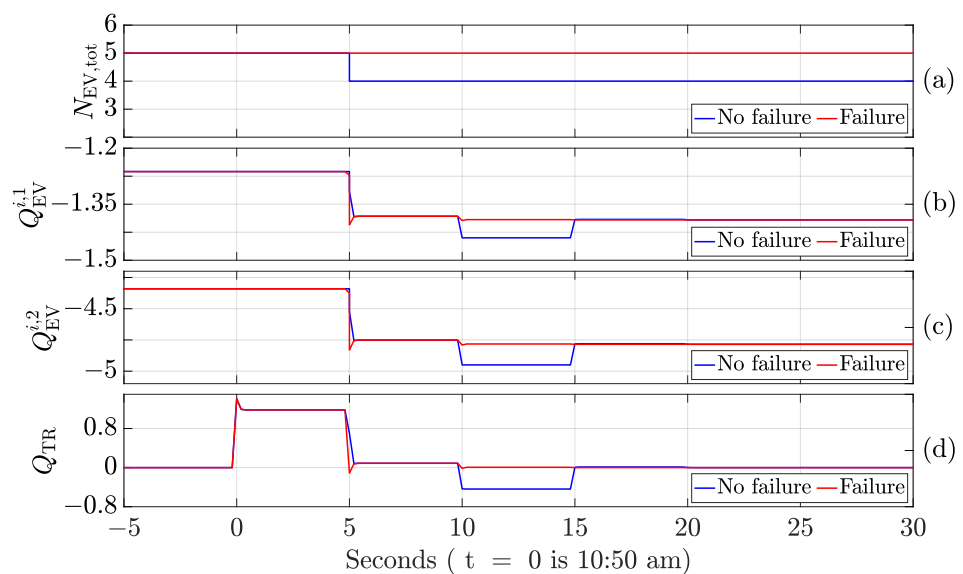


Figure 17. System response without and with communication failure case 1, (a) number of EVs present; (b)  $Q$  supplied by an online EV at Level 1 in kVAR; (c)  $Q$  supplied by an online EV at Level 2 in kVAR; (d) transformer reactive power in kVAR.

First, without communication failure- The EV-10 leaves the system at  $t = 0$ , and therefore does not execute the command sent by the controller at  $t = -5$ . Thus, at  $t = 5$ , in addition to a reduction in  $N_{EV,tot}$ , the controller also tracks a positive  $Q_{TR}$ . This results in overcompensation at  $t = 10$ , which is adjusted by the controller in the next few execution cycles. However, with communication failure, at  $t = 0$ , the controller computes a larger  $N_{EV,tot}$  than actual, and computes lower than required  $Q_{EV}^{i,a}$  values for total compensation. At  $t = 5$ , the controller tracks the same  $N_{EV,tot}$  as  $t = 0$  and only compensates for the under-compensation at  $t = 5$ , which is fully corrected by  $t = 10$ . As shown in Figure 17b–d by  $t = 15$ ,  $Q_{EV}^{i,1}$ ,  $Q_{EV}^{i,2}$ , and  $Q_{TR}$  are same as it is in the case with no communication failure. Notably, the controller is able to ride through this failure. Moreover, the communication delay has no consequential impact on the controller's stability.

### 5.7.2. Communication Failure Case 2

In this case, a communication failure occurs abruptly when an online EV stops receiving  $Q_{EV}^{i,a}$  signal from the controller. Upon failure, the EV enters a wait period in anticipation of the restoration of correct communication before disengaging from reactive power compensation. During the wait period, the EV supplies reactive power at the last received controller command. In this study, the wait period is assumed to be 5 controller execution cycles, i.e., 25 s.

For discussion, this communication failure is assumed to occur between EV-2 and the controller at  $t = 0$ . It is assumed that the communication is not restored during the wait period. After entering its wait period, EV-2 supplies the last received  $Q_{EV}^{2,2}$  for the next 5 cycles i.e., till  $t = 25$ . The controller, unaware of reactive power supply from EV-2, at  $t = 5$  tracks a decrease in  $N_{EV,tot}$  as shown in Figure 18a. To make the tracking error zero, the controller generates new increased  $Q_{EV}^{i,a}$  references for the online EVs which results in overcompensation at  $t = 10$ . In the next couple of execution cycles, the controller fixes the overcompensation. At  $t = 20$ , it can be seen that  $Q_{EV}^{i,a}$  is the same as the no-failure case. But, this is disrupted when at the end of wait period at  $t = 25$ , EV-2 disconnects from the system, i.e.,  $Q_{EV}^{2,2}$  becomes 0. The tracking error becomes positive which is compensated for by the controller at  $t = 30$ . The online EVs are now operating at their limits to compensate for positive  $Q_{TR}$ . It can be concluded that the controller is robust to this communication failure scenario as well. The EV supplying the last received  $Q_{EV}^{i,a}$  value during its wait period is equivalent to an external disturbance in the system which is compensated for by the controller.

### 5.7.3. Communication Failure Case 3

In this case, similar to Case 2, a communication failure occurs abruptly where an online EV stops receiving  $Q_{EV}^{i,a}$  signal from the controller. However, unlike Case 2, the EV continues to supply reactive power at the last received controller command till it goes offline or communication is restored.

For discussion, the same system conditions as Case 2 are considered. At  $t = 0$ , the communication link between EV-2 and the controller breaks abruptly. It is assumed that for the next 10 min (=600 s) the communication is not restored. Therefore, EV-2 continues supplying reactive power at the last received controller command  $Q_{EV}^{2,2}$  as shown in Figure 19d till the communication is restored. Since the controller is unaware of EV-2's presence, at  $t = 5$ , it detects a decrease in  $N_{EV,tot}$ . Therefore the controller generates new increased  $Q_{EV}^{i,a}$  references for the four online EVs, which in addition to EV-2's supply, results in overcompensation at  $t = 10$ . As the controller fixes the overcompensation by  $t = 20$ , it can be seen that  $Q_{EV}^{i,a}$  is the same as the case without failure. It can be concluded that the controller is able to compensate for this communication failure case as well.

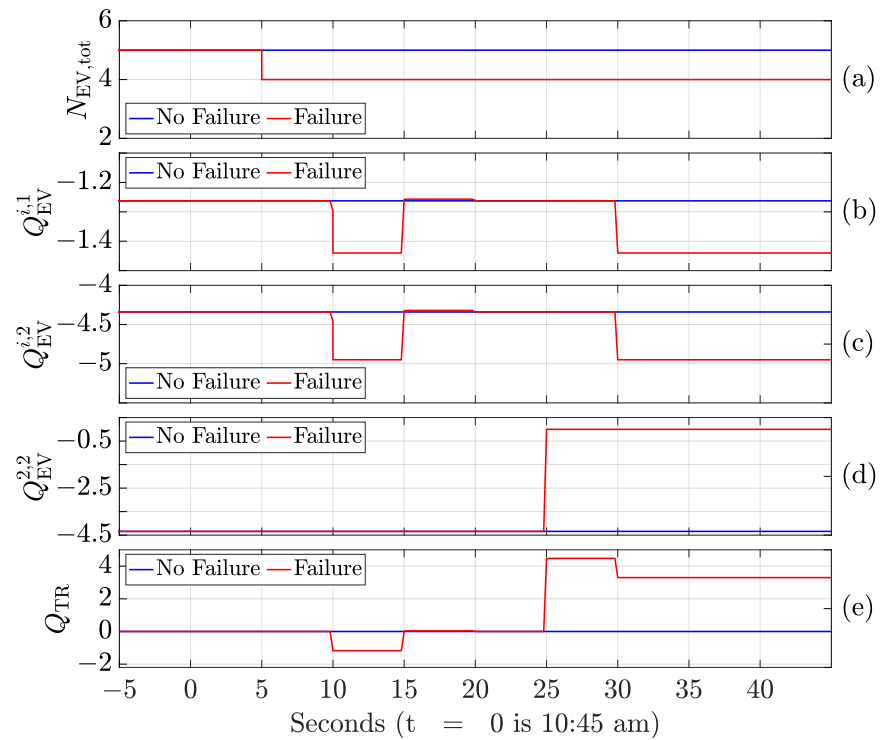


**Figure 18.** System response without and with communication failure case 2, (a) number of EVs present; (b)  $Q$  supplied by an online EV at Level 1 in kVAR; (c)  $Q$  supplied by an online EV at Level 2 in kVAR; (d)  $Q$  supplied by EV-2 at Level 2 in kVAR; (e) transformer reactive power in kVAR.

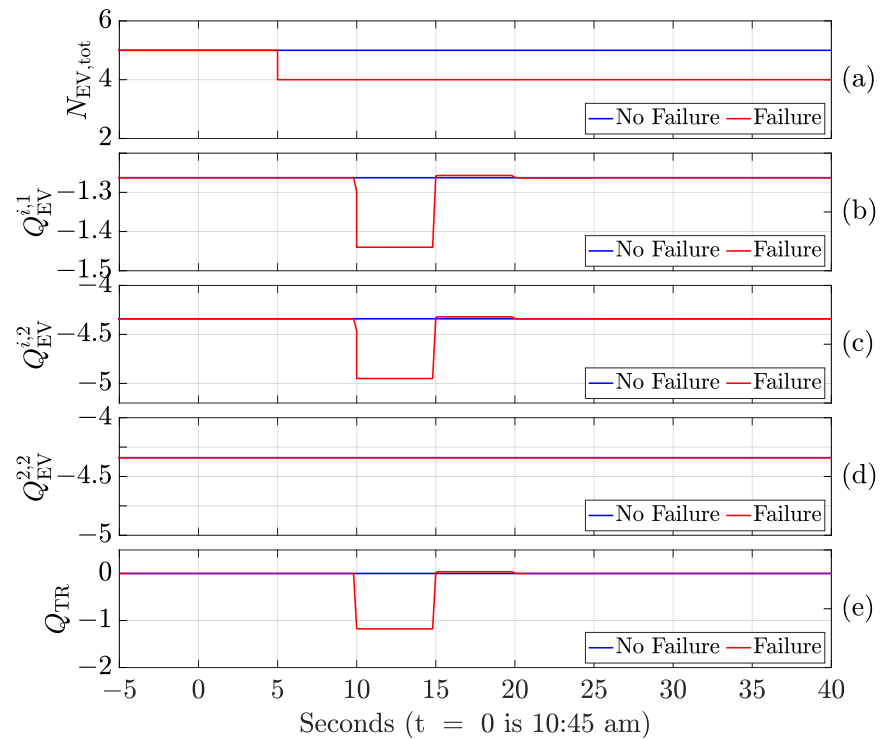


**Figure 19.** System response without and with communication failure case 3, (a) number of EVs present; (b)  $Q$  supplied by an online EV at Level 1 in kVAR; (c)  $Q$  supplied by an online EV at Level 2 in kVAR; (d)  $Q$  supplied by EV-2 at Level 2 in kVAR; (e) transformer reactive power in kVAR.

## 6. Conclusions

This paper proposes a practical technique for mitigating low-voltage distribution transformer overloading due to increasing residential EV charging power demand. First, a qualitative and quantitative study to show the impact of increased EV charging demand on distribution transformers is presented for four diversified EV charging scenarios. Thereafter, IEEE Standard C57.91-2011 is used to quantify the impact of EV charging on the transformer insulation life. It is shown that increased EV penetration significantly impacts transformer life in all charging scenarios. Subsequently, a centralized recursive controller that periodically sets reactive power references for EVs to supply local reactive power is proposed. The controller's stability and robustness to system communication delays and failures are also discussed. It is shown that with the proposed technique distribution transformer's life increases by an average of nearly 47% in all four scenarios. In addition, with consideration of seasonal variations in load demand, and ambient temperatures, the annual transformer aging is calculated, and it is shown that with the proposed method, the transformer life improves by nearly an average of 49% compared to the uncompensated case. The results indicate that the proposed controller can successfully regulate and minimize the distribution transformer's reactive power flow and therefore extend its life and is stable under different operation scenarios. It ensures end-user convenience and can be conveniently adopted by transformers in power grids without significant infrastructure upgrades. In the future, this work can be experimentally verified with appropriate resources, and possible practical challenges be studied.

**Author Contributions:** Conceptualization, A.J. and M.K.-G.; methodology, A.J. and M.K.-G.; software, A.J.; validation, A.J. and M.K.-G.; formal analysis, A.J. and M.K.-G.; investigation, A.J. and M.K.-G.; resources, M.K.-G.; writing—original draft preparation, A.J.; writing—review and editing, M.K.-G.; supervision, M.K.-G. All authors have read and agreed to the published version of the manuscript.

**Funding:** This research received no external funding.

**Institutional Review Board Statement:** Not applicable.

**Informed Consent Statement:** Not applicable.

**Data Availability Statement:** Not applicable.

**Conflicts of Interest:** The authors declare no conflict of interest.

## References

1. Hu, L.; Dong, J.; Lin, Z. Modeling charging behavior of battery electric vehicle drivers: A cumulative prospect theory based approach. *Transp. Res. Part C Emerg. Technol.* **2019**, *102*, 474–489. [CrossRef]
2. Ashtari, A.; Bibeau, E.; Shahidinejad, S.; Molinski, T. PEV Charging Profile Prediction and Analysis Based on Vehicle Usage Data. *IEEE Trans. Smart Grid* **2012**, *3*, 341–350. [CrossRef]
3. Ricardo Inc. (Report). EV Consumer Behavior, Fuels Institute, Report, June 2021, MI, USA. Available online: <https://www.fuelsinstitute.org/Research/Reports/EV-Consumer-Behavior/EV-Consumer-Behavior-Report.pdf> (accessed on 26 November 2022).
4. Smart, J.G.; Salisbury, S.D. *Plugged In: How Americans Charge Their Electric Vehicles*; Idaho National Lab. (INL): Idaho Falls, ID, USA, 2015. Available online: <https://www.osti.gov/biblio/1369632> (accessed on 26 November 2022).
5. Bunga, S.K.; Eltom, A.H.; Sisworahardjo, N. Impact of Plug-in Electric Vehicle battery charging on a distribution system. In Proceedings of the 2014 IEEE Industry Application Society Annual Meeting, Vancouver, BC, Canada, 5–9 October 2014; pp. 1–5.
6. Awadallah, M.A.; Singh, B.N.; Venkatesh, B. Impact of EV Charger Load on Distribution Network Capacity: A Case Study in Toronto. *Can. J. Electr. Comput. Eng.* **2016**, *39*, 268–273. [CrossRef]
7. Erden, F.; Kisacikoglu, M.C.; Gurec, O.H. Examination of EV-grid integration using real driving and transformer loading data. In Proceedings of the 2015 9th International Conference on Electrical and Electronics Engineering (ELECO), Bursa, Turkey, 26–28 November 2015; pp. 364–368.
8. Sausen, J.P.; Abaide, A.R. Evaluation of Electric Vehicle Charging on Distribution Transformer Loading. In Proceedings of the 2018 IEEE PES Transmission Distribution Conference and Exhibition—Latin America (T D-LA), Lima, Peru, 18–21 September 2018; pp. 1–5.

9. Satarworn, S.; Hoonchareon, N. Impact of EV home charger on distribution transformer overloading in an urban area. In Proceedings of the 14th International Conference on Electrical Engineering/Electronics, Computer, Telecommunications and Information Technology (ECTI-CON), Phuket, Thailand, 27–30 June 2017; pp. 469–472.
10. Wamburu, J.; Lee, S.; Shenoy, P.; Irwin, D. Analyzing Distribution Transformers at City Scale and the Impact of EVs and Storage. In Proceedings of the Ninth International Conference on Future Energy Systems, Karlsruhe, Germany, 12–15 June 2018; pp. 157–167.
11. Rutherford, M.J.; Yousefzadeh, V. The impact of Electric Vehicle battery charging on distribution transformers. In Proceedings of the 2011 Twenty-Sixth Annual IEEE Applied Power Electronics Conference and Exposition (APEC), Fort Worth, TX, USA, 6–11 March 2011; pp. 396–400.
12. Assolami, Y.O.; Morsi, W.G. Impact of Second-Generation Plug-In Battery Electric Vehicles on the Aging of Distribution Transformers Considering TOU Prices. *IEEE Trans. Sustain. Energy* **2015**, *6*, 1606–1614. [[CrossRef](#)]
13. Ko, E.; Dokic, T.; Kezunovic, M. Prediction Model for the Distribution Transformer Failure Using Correlation of Weather Data. In Proceedings of the 5th International Colloquium on Transformer Research and Asset Management, Opatija, Croatia, 9–12 October 2019; pp. 135–144.
14. Ye, Z.; Wu, K.; Cheng, C.; Song, W. Replacement of aging power transformers considering system risks under multi-level load. In Proceedings of the 2017 IEEE Power Energy Society General Meeting, Chicago, IL, USA, 16–20 July 2017; pp. 1–5.
15. Dubey, A.; Santoso, S. Electric Vehicle Charging on Residential Distribution Systems: Impacts and Mitigations. *IEEE Access* **2015**, *3*, 1871–1893. [[CrossRef](#)]
16. Limmer, S. Dynamic pricing for electric vehicle charging—A literature review. *Energies* **2019**, *12*, 3574. [[CrossRef](#)]
17. Davis, B.M.; Bradley, T.H. The Efficacy of Electric Vehicle Time-of-Use Rates in Guiding Plug-in Hybrid Electric Vehicle Charging Behavior. *IEEE Trans. Smart Grid* **2012**, *3*, 1679–1686. [[CrossRef](#)]
18. Dubey, A.; Santoso, S.; Cloud, M.P.; Waclawiak, M. Determining Time-of-Use Schedules for Electric Vehicle Loads: A Practical Perspective. *IEEE Power Energy Technol. Syst. J.* **2015**, *2*, 12–20. [[CrossRef](#)]
19. Shao, S.; Zhang, T.; Pipattanasomporn, M.; Rahman, S. Impact of TOU rates on distribution load shapes in a smart grid with PHEV penetration. In Proceedings of the IEEE PES Transmission and Distribution Conference and Exposition, New Orleans, LA, USA, 19–22 April 2010; pp. 1–6.
20. Pradhan, P.; Ahmad, I.; Habibi, D.; Kothapalli, G.; Masoum, M. Reducing the Impacts of Electric Vehicle Charging on Power Distribution Transformers. *IEEE Access* **2020**, *8*, 210183–210193. [[CrossRef](#)]
21. Zheng, Y.; Luo, J.; Yang, X.; Yang, Y. Intelligent Regulation on Demand Response for Electric Vehicle Charging: A Dynamic Game Method. *IEEE Access* **2020**, *8*, 66105–66115. [[CrossRef](#)]
22. Dang, Q.; Wu, D.; Boulet, B. EV Charging Management with ANN-Based Electricity Price Forecasting. In Proceedings of the IEEE Transportation Electrification Conference & Expo (ITEC), Chicago, IL, USA, 23–26 June 2020; pp. 626–630.
23. Zheng, Y.; Niu, S.; Shang, Y.; Shao, Z.; Jian, L. Integrating plug-in electric vehicles into power grids: A comprehensive review on power interaction mode, scheduling methodology and mathematical foundation. *Renew. Sustain. Energy Rev.* **2019**, *112*, 424–439. [[CrossRef](#)]
24. Shao, S.; Pipattanasomporn, M.; Rahman, S. Demand Response as a Load Shaping Tool in an Intelligent Grid With Electric Vehicles. *IEEE Trans. Smart Grid* **2011**, *2*, 624–631. [[CrossRef](#)]
25. Nimalsiri, N.; Ratnam, E.; Smith, D.; Mediwaththe, C.; Halgamuge, S. Coordinated Charge and Discharge Scheduling of Electric Vehicles for Load Curve Shaping. *IEEE Trans. Intell. Transp. Syst.* **2021**, *23*, 1–13. [[CrossRef](#)]
26. Deilami, S.; Masoum, A.S.; Moses, P.S.; Masoum, M.A.S. Real-Time Coordination of Plug-In Electric Vehicle Charging in Smart Grids to Minimize Power Losses and Improve Voltage Profile. *IEEE Trans. Smart Grid* **2011**, *2*, 456–467. [[CrossRef](#)]
27. Shang, Y.; Liu, M.; Shao, Z.; Jian, L. Internet of smart charging points with photovoltaic Integration: A high-efficiency scheme enabling optimal dispatching between electric vehicles and power grids. *Appl. Energy* **2020**, *278*, 115640. [[CrossRef](#)]
28. Beaude, O.; Lasaulce, S.; Hennebel, M.; Mohand-Kaci, I. Reducing the Impact of EV Charging Operations on the Distribution Network. *IEEE Trans. Smart Grid* **2016**, *7*, 2666–2679. [[CrossRef](#)]
29. Blonsky, M.; Munankarmi, P.; Balamurugan, S.P. Incorporating Residential Smart Electric Vehicle Charging in Home Energy Management Systems. In Proceedings of the IEEE Green Technologies Conference (GreenTech), Denver, CO, USA, 7–9 April 2021; pp. 187–194.
30. Jain, A.; Karimi-Ghartemani, M. Reducing the Impact of Plug-in Electric Vehicles on Distribution Transformers. In Proceedings of the IEEE Energy Conversion Congress and Exposition (ECCE), Detroit, MI, USA, 11–15 October 2020; pp. 878–884.
31. Muratori, M. Impact of Uncoordinated Plug-in Electric Vehicle Charging on Residential Power Demand—Supplementary Data. National Renewable Energy Laboratory. 2017. Available online: <https://data.nrel.gov/submissions/69> (accessed on 26 November 2022).
32. C57.91-2011; IEEE Guide for Loading Mineral-Oil-Immersed Transformers and Step-Voltage Regulators. IEEE Std (Revision of IEEE Std C57.91-1995); IEEE: Manhattan, NY, USA, 2012; pp. 1–123.
33. Yilmaz, M.; Krein, P.T. Review of Battery Charger Topologies, Charging Power Levels, and Infrastructure for Plug-In Electric and Hybrid Vehicles. *IEEE Trans. Power Electron.* **2013**, *28*, 2151–2169. [[CrossRef](#)]
34. Willis, L. *Power Distribution Planning Reference Book*, 2nd ed.; CRC Press: Boca Raton, FL, USA, 2004.
35. Kersting, W.H. Center tapped transformer and 120/240 volt secondary models. In Proceedings of the 2008 IEEE Rural Electric Power Conference, Charleston, SC, USA, 27–29 April 2008; pp. 1–7.

36. Muratori, M.; Roberts, M.C.; Sioshansi, R.; Marano, V.; Rizzoni, G. A highly resolved modeling technique to simulate residential power demand. *Appl. Energy* **2013**, *107*, 465–473. [CrossRef]
37. Muratori, M.; Marano, V.; Sioshansi, R.; Rizzoni, G. Energy consumption of residential HVAC systems: A simple physically-based model. In Proceedings of the IEEE Power and Energy Society General Meeting, San Diego, CA, USA, 22–26 July 2012; pp. 1–8.
38. Muratori, M.; Moran, M.J.; Serra, E.; Rizzoni, G. Highly-resolved modeling of personal transportation energy consumption in the United States. *Energy* **2013**, *58*, 168–177. [CrossRef]
39. 2013, B. NLG6—On-Board-Fast Charger. Available online: <https://www.speakev.com/attachments/brusa-data-sheet-pdf.1232/> (accessed on 26 November 2022).
40. NFPA 70: National Electrical Code (NEC). 2014. Available online: [https://site.ieee.org/icps-ehe/files/2015/11/13-9-NFPA-70\\_-National-Electrical-Code-NEC-Article-220.pdf](https://site.ieee.org/icps-ehe/files/2015/11/13-9-NFPA-70_-National-Electrical-Code-NEC-Article-220.pdf) (accessed on 26 November 2022).
41. San Diego Gas and Electric. Electric Distribution Design Manual. Technical Report. 2019. Available online: <https://www.sdge.com/sites/default/files/DM.pdf> (accessed on 26 November 2022).
42. Kersting, W.H. *Distribution System Modeling and Analysis*, 3rd ed.; CRC Press: Boca Raton, FL, USA, 2012.
43. Sen, P.K.; Pansuwan, S.; Malmedal, K.; Martinoo, O.; Simoes, M.G. *Transformer Overloading and Assessment of Loss-of-Life for Liquid-Filled Transformers*; Technical report; Power Systems Engineering Research Center: Tempe, AZ, USA, 2011. Available online: [https://pserc.wisc.edu/wp-content/uploads/sites/755/2018/08/T-25\\_Final-Report\\_Feb-2011.pdf](https://pserc.wisc.edu/wp-content/uploads/sites/755/2018/08/T-25_Final-Report_Feb-2011.pdf) (accessed on 26 November 2022).
44. Kisacikoglu, M.C.; Ozpineci, B.; Tolbert, L.M. Reactive power operation analysis of a single-phase EV/PHEV bidirectional battery charger. In Proceedings of the 8th International Conference on Power Electronics—ECCE Asia, Jeju, Republic of Korea, 30 May–3 June 2011; pp. 585–592.
45. Abeywardana, D.B.W.; Acuna, P.; Hredzak, B.; Aguilera, R.P.; Agelidis, V.G. Single-Phase Boost Inverter-Based Electric Vehicle Charger With Integrated Vehicle to Grid Reactive Power Compensation. *IEEE Trans. Power Electron.* **2018**, *33*, 3462–3471. [CrossRef]
46. Yu, H.; Niu, S.; Shang, Y.; Shao, Z.; Jia, Y.; Jian, L. Electric vehicles integration and vehicle-to-grid operation in active distribution grids: A comprehensive review on power architectures, grid connection standards and typical applications. *Renew. Sustain. Energy Rev.* **2022**, *168*, 112812. [CrossRef]
47. Kempton, W.; Tomić, J. Vehicle-to-grid power fundamentals: Calculating capacity and net revenue. *J. Power Sources* **2005**, *144*, 268–279. [CrossRef]
48. Gowri, K.; Pratt, R.M.; Tuffner, F.K.; Kintner-Meyer, M.C. Vehicle to Grid Communication Standards Development, Testing and Validation—Status Report. 2011. Available online: [https://www.pnnl.gov/main/publications/external/technical\\_reports/PNNL-20844.pdf](https://www.pnnl.gov/main/publications/external/technical_reports/PNNL-20844.pdf) (accessed on 26 November 2022).
49. Jury, E.I. A Simplified Stability Criterion for Linear Discrete Systems. *Proc. IRE* **1962**, *50*, 1493–1500. [CrossRef]
50. SAE International. *Use Cases for Communication Between Plug-in Vehicles and the Utility Grid. Surface Vehicle Information Report-SAE J2836-1*; Technical report; SAE International: Detroit, MI, USA, 2010.